



Mathematical modeling and simulation of thermal management in polymer electrolyte membrane fuel cell stacks



Amir Amirfazli^a, Saeed Asghari^{b,*}, Morteza Koosha^b

^a Mechanical Engineering Department, Isfahan University of Technology, Isfahan, Iran

^b Institute of Materials and Energy, Iranian Space Research Center, Isfahan, Iran

HIGHLIGHTS

- Thermal management in PEM fuel cell stacks are modeled through a mathematical model.
- Thermal management of stacks with U and Z configurations are compared to each other.
- Increasing coolant flow rate and manifold sizes will increase temperature uniformity.
- The Z configuration is not appropriate for stacks with very small manifold sizes.

ARTICLE INFO

Article history:

Received 18 December 2013

Received in revised form

12 May 2014

Accepted 13 June 2014

Available online 21 June 2014

Keywords:

Polymer electrolyte membrane (PEM) fuel cell

Stack

Cooling flow field

Temperature distribution

Manifold

Coolant

ABSTRACT

The narrow range of operating temperature and small temperature differences between the stack and the ambient have made the fuel cell thermal management as one of the key factors that influence the performance and durability of polymer electrolyte membrane fuel cell (PEMFC) stacks. In the present study, an analytical model is developed to investigate coolant flow and temperature distributions within a PEMFC stack. The model consists of a coolant flow distribution submodel and a thermal submodel for determination of coolant mass flow distribution between different cooling flow fields of the stack and the temperature distribution within the stack, respectively. The coolant mass flow rate and the temperature distributions in stacks with U and Z configurations are compared with each other using the developed model. The test results of two 65-cells stacks are presented to verify the simulation. The results indicate that the Z configuration results in more uniform temperature distribution than the U configuration in low values of the manifold cross sectional area. However, the Z configuration cannot be applied in the stacks with very small manifold sizes. A parametric analysis is also conducted to assess the effects of some parameters on the temperature distribution in a stack.

© 2014 Elsevier B.V. All rights reserved.

1. Introduction

With the advantages of low working temperature, high power density, quick start up, transient ability and low emissions features PEM fuel cells is considered to be the most promising candidate for the next generation power source for transportation, stationary, auxiliary and portable applications [1–4]. Despite of wide researches and progressions on fuel cells, several technical barriers to their commercialization still exist, especially about their durability

and cost. There is a significant amount of heat generation in the fuel cell stack due to electrochemical reactions and electrical resistances. The heat generated is comparable to electrical power output and should be removed efficiently to avoid overheating of the components and guarantees the favorable working temperature range for the current PEMFCs which is usually in the range of 60–80 °C. Improper thermal management and non-uniform temperature distribution within the fuel cell stack may cause electrolyte drying (global or local) or electrode flooding which both lower the fuel cell performance [5–7]. On the other hand, the temperature difference between the PEMFC and the ambient is very small in comparison with the internal combustion engines. Thus, a proper thermal management for PEMFC stack is very challenging, particularly in automotive applications which require stacks with high power output and high power density.

* Corresponding author. Institute of Materials and Energy, Iranian Space Research Center, 7th kilometer of Imam, Khomeini Ave., P.O. Box 81955-174, Isfahan, Iran. Tel.: +98 31 33222428; fax: +98 31 33222446.

E-mail addresses: amir.mec.iut@outlook.com (A. Amirfazli), asghari@fuelcell.ir, asghari@me.iut.ac.ir (S. Asghari).

Nomenclature			
ΔP_{st}	pressure drop due to splitting or combining of two streams in a manifold segment	Re_m	Reynolds number of coolant flow in a manifold segment
ΔP_c	pressure drop due to divergence or convergence of two streams in T shape section of a cell	f_m	friction coefficient in a manifold segment
ΔP_{f-b}	pressure drop due to friction and bending in a cooling flow field channel	U_{ch}	coolant flow velocity in a cooling flow field channel
ΔP_{fm}	pressure drop due to friction in manifolds	Q_c	coolant flow rate of a cell
R_{st}	hydraulic resistance related to splitting or combining of coolant flow in manifold segments	A_{ch}	cross sectional area of a cooling flow field channel
R_c	hydraulic resistance related to divergence or convergence of coolant stream in T shape section of a cell	z	number of channels in cooling flow field of a cell
ΔP_m	total pressure drop in a manifold segment	ΔP_{cell}	total pressure drop in cooling flow field of a cell
ΔP_{en}	pressure drop due to contraction of coolant flow in inlet section of a cell	Fr	relaxation coefficient
ΔP_{ex}	pressure drop due to expansion of coolant flow in outlet section of a cell	Q_{corr}	corrected coolant flow rate of a cell before relaxing
R_{en}	hydraulic resistance related to contraction of flow in inlet section of a cell	U_{corr}	corrected velocity of coolant flow in a cooling flow field channel
R_{ex}	hydraulic resistance related to expansion of flow in outlet section of a cell	Q	heat generation per cell
N	number of cells	V	cell working voltage
M	number of nodes in cooling flow field channels	I	output electrical current of stack
U_m	coolant flow velocity in a manifold segment	T_m	coolant mean temperature of inlet and outlet section of a cell
ρ	coolant density	q''_{ch}	surface heat flux of a cooling flow field channel
μ	coolant dynamic viscosity	$T_s(x)$	surface temperature of a cooling flow field channel
L	length of manifold segment	IUT	index of uniform temperature
A_m	manifold cross sectional area	A_{sa}	surface area of a cooling flow field channel
Q_m	volumetric flow rate of coolant in a manifold segment	q_{ch}	contribution of a flow field channel from generated heat in its related cell
R_{fm}	hydraulic resistance related to friction in a manifold segment	P	perimeter of a cooling flow field channel
D_{hm}	hydraulic diameter of manifolds	c_p	specific heat capacity of coolant
		x	distance from the channel inlet along a cooling flow field channel
		h	convective heat transfer coefficient
		\dot{m}_{ch}	coolant mass flow rate in a cooling flow field channel
		\bar{T}	average temperature of a stack
		$T_{ch,i}$	temperature at inlet section of a cooling flow field channel
		$T_{ch,o}$	temperature at outlet section of a cooling flow field channel

Essentially, the issue of thermal management in fuel cell stack can be viewed at two levels; at the cell level to ensure proper membrane hydration and thereby ensure good conductivity of the membrane, and at the system level to ensure temperature uniformity along the stack and keep the stack from heating up [8].

A number of studies have been conducted on the thermal management issue in the PEM fuel cells. In contrast with the extensive single cell models available in literature, limited number of studies is available for the modeling and simulation of cooling behavior of PEM fuel cell stacks. Most of the studies are devoted to modeling of cooling channel on bipolar plates, investigation of various cooling strategies and selection of an appropriate cooling method.

Yu and Jung proposed a thermal management strategy of a PEMFC system with a large active area for transportation applications [9]. Their model was composed of different sub-models for the water transport through the MEA, the electrochemical reaction in the cathode catalyst layer and the two-dimensional temperature distribution within the fuel cell. They concluded that the fuel cell operating temperature can be effectively controlled by adjusting cooling fan operation.

In another study by Asghari et al., design of cooling flow field as well as thermal management subsystem of a 5 kW PEM fuel cell system were investigated [7]. The number of parallel channels in the parallel serpentine flow field was selected as the design parameter and its optimum value was obtained by compromising between the minimum pressure drop of coolant across the flow

field and the maximum temperature uniformity within the bipolar plate.

López-Sabirón et al. used a theoretical 1D model, based on electrochemical and thermal equations, to estimate the performance of open-cathode PEM fuel cells as well as to define an optimum cooling system and channel geometry for the cathode side [1].

Sasmitho et al. carried out a computational study of PEFC stacks with various cooling strategies. It was shown that liquid cooling yields best performance among the alternative designs examined [10].

Park and Li developed a non-isothermal stack model to analyze the effects of flow variance and temperature distribution on the performance of a PEMFC stack [11]. The stack model consists of the flow network solver for pressure and mass flow distributions for the reactant gas streams and cooling water, and the heat transfer solver for temperature distribution among the cells in the stack. It is shown that the effect of temperature is dominant on the cell voltage variance when the flow variance is small for sufficiently uniform distribution of reactant flow among the cells in the stack. Furthermore they concluded that flow and temperature distribution have a different influence, and a judicious matching of their distribution can provide the ideal uniform cell voltage distribution.

As a rule of thumb, PEM fuel cell stacks above 5 kW should be water cooled, those below 2 kW air cooled, with a decision for stacks in between being a matter of judgment [12,13]. One of the problems encountered when stacking fuel cells is a non-uniform

coolant flow distribution between cooling flow fields of cells, which causes an uneven temperature distribution within the stack. Therefore, geometrical design of the cooling flow field and manifolds are important issues to be considered.

In the present paper, an analytical model including two sub-models is developed to study the coolant flow and temperature distribution within a water-cooled PEM fuel cell stack. The coolant flow distribution submodel determines the distribution of coolant flow between different cells in the stack. With considering heat generation in each cell and using the results of the flow distribution submodel, the thermal submodel yields the temperature distribution within the fuel cell stack. The U and Z stack configurations are investigated and compared to each other through the analytical model. The results of the thermal submodel are verified by some experimental data. Finally, a parametric study is conducted to investigate the effect of some main parameters on the temperature uniformity in the fuel cell stack.

2. Analytical model

The analytical model consists of two main submodels: (1) a coolant flow distribution model, which is used to determine the mass flow distribution of coolant between different cooling flow fields of the fuel cell stack; and (2) a thermal model, which computes the coolant temperature increase along the flow field and also the temperature distribution within the fuel cell stack.

By the coolant flow distribution submodel, the flow distribution is calculated using the Bernoulli equation and the fuel cell stack is modeled as a network of hydraulic resistances in parallel and in series; describing the resistances in the cooling flow fields and in the manifolds (Fig. 1). As indicated in Fig. 1, two flow patterns are considered in the current analysis: U-configuration and Z-configuration.

2.1. Coolant flow distribution submodel

The coolant flow and pressure distributions are determined using an iterative approach. A systematic algorithm is constructed based on the assumption that the flow distribution in the fuel cell stack can be modeled by means of hydraulic resistances in the manifold and in the cooling flow fields. In other words, the stack is represented as a network of hydraulic resistances, in parallel and in series as shown in Fig. 1.

In the following, the pressure drops included in the model are described and the solution algorithm is explained in detail. The pressure drops included in the analytical model are divided into four classes:

1. The pressure drop due to splitting and combining of two streams in the inlet and outlet manifolds (ΔP_{st-in} , ΔP_{st-out})
2. The pressure drop due to friction of flow in the inlet and outlet manifolds (ΔP_{fm-in} , ΔP_{fm-out})

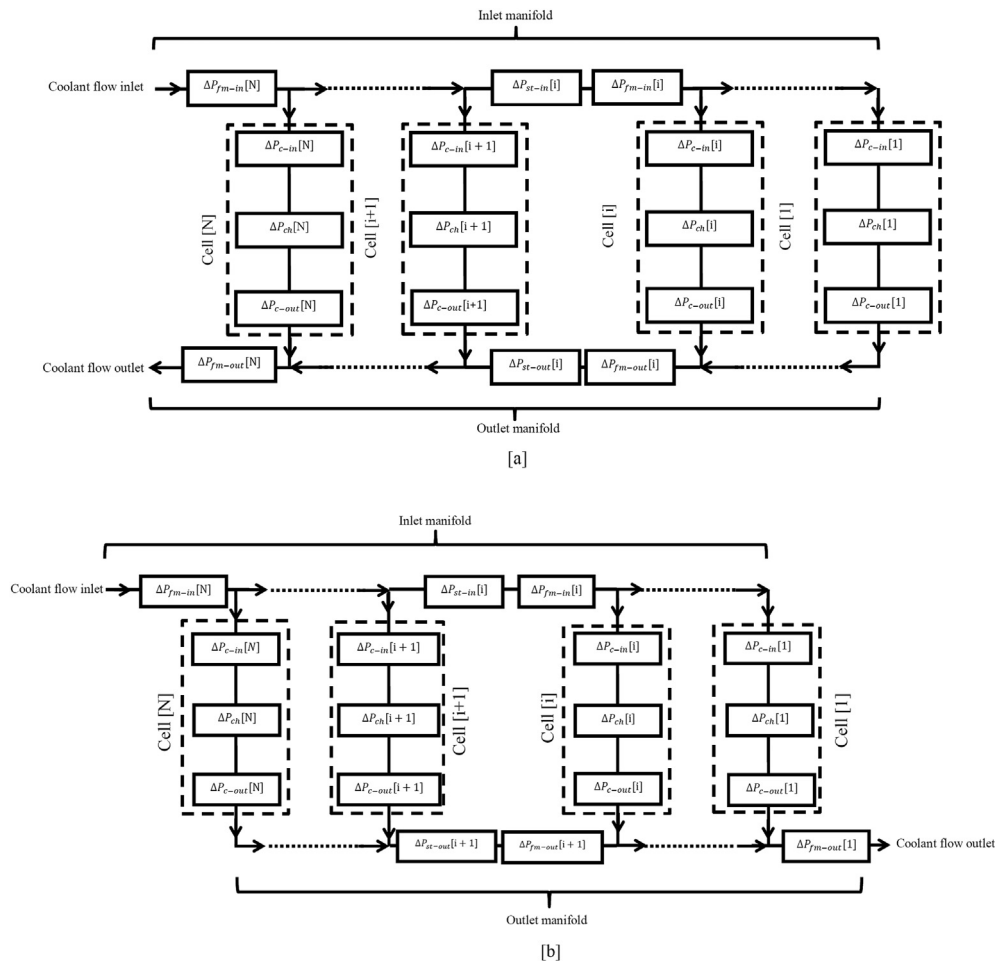


Fig. 1. Network of hydraulic resistances; (a) U configuration and (b) Z configuration.

3. The losses caused by deflection of the main stream in the manifold into or out of the cells (ΔP_{c-in} , ΔP_{c-out})
4. The losses related to the cooling flow field channels which consist of:
 - a) Pressure drop due to the effects of friction and bending
 - b) Pressure drop caused by expansion and contraction of the main stream into or out of the channels.

2.1.1. Pressure drop due to splitting and combining of two streams in the inlet and outlet manifolds

The shape of the junctions between the manifolds and the diffuser part in the cooling flow field of the cells are approximated to a converging/diverging T shape for which the pressure drop relations are obtained from IDELCHICK's hydraulic resistances handbook [14].

These pressure drops are determined by using the following relations:

$$\Delta P_{st-in}[i] = 0.5 \cdot R_{st-in}[i] \cdot \rho \cdot U_{m-in}[i]^2 \quad (1a)$$

$$U_{m-in}[i] = \frac{Q_{m-in}[i]}{A_{m-in}} \quad (1b)$$

$$\Delta P_{st-out}[i] = 0.5 \cdot R_{st-out}[i] \cdot \rho \cdot U_{m-out}[i]^2 \quad (2a)$$

$$U_{m-out}[i] = \frac{Q_{m-out}[i]}{A_{m-out}} \quad (2b)$$

where $U_{m-in}[i]$ and $U_{m-out}[i]$ are coolant flow velocities in ith segment of the manifolds, $R_{st-in}[i]$ and $R_{st-out}[i]$ are hydraulic resistances related to splitting and combining of coolant flow in the inlet and the outlet manifolds, A_{m-in} and A_{m-out} are the cross sectional areas of the manifolds, and $Q_{m-in}[i]$ and $Q_{m-out}[i]$ are the volumetric flow rates of the coolant in ith segment of the manifolds.

The resistance coefficients due to splitting and combining of the fluid streams (R_{st-in} , R_{st-out}) are related to the flow ratios between the flow in the manifolds and in the cells. These relations are shown in Table 1. In the cases where explicit relations for hydraulic resistances are not available, a correlation is obtained using curve fitting of data available in IDELCHICK's hydraulic resistances handbook [14].

2.1.2. Friction losses in the manifolds

The coolant flow in the manifolds is simulated as a flow in a conduit. With this assumption, the pressure drop can be determined by conventional internal fluid flow relations [15]. The amount of pressure drop due to friction in ith segment of the inlet manifold is determined based on the following correlations:

$$\Delta P_{fm-in}[i] = 0.5 \cdot R_{fm-in}[i] \cdot \rho \cdot U_{m-in}[i]^2 \quad (3a)$$

$$R_{fm-in}[i] = f_{m-in}[i] \times \frac{L}{D_{hm-in}} \quad (3b)$$

$$f_{m-in}[i] = \begin{cases} 64/Re_{m-in}[i] & Re_{m-in} < 2100 \\ 0.316/Re_{m-in}[i]^{0.25} & Re_{m-in} > 2100 \end{cases} \quad (3c)$$

$$Re_{m-in}[i] = \frac{\rho U_{m-in}[i] D_{hm-in}}{\mu} \quad (3d)$$

where $Re_{m-in}[i]$ is the Reynolds number, $f_{m-in}[i]$ the friction coefficient and D_{hm-in} and μ are hydraulic diameter and dynamic viscosity of the coolant, respectively.

The amount of pressure drop due to friction in ith segment of the outlet manifold is determined using the following correlations:

$$\Delta P_{fm-out}[i] = 0.5 \cdot R_{fm-out}[i] \cdot \rho \cdot U_{m-out}[i]^2 \quad (4a)$$

$$R_{fm-out}[i] = f_{m-out} \times \frac{L}{D_{hm-out}} \quad (4b)$$

$$f_{m-out} = \begin{cases} 64/Re_{m-out}[i] & Re_{m-out} < 2100 \\ 0.316/Re_{m-out}[i]^{0.25} & Re_{m-out} > 2100 \end{cases} \quad (4c)$$

$$Re_{m-out}[i] = \frac{\rho U_{m-out}[i] D_{hm-out}}{\mu} \quad (4d)$$

2.1.3. The losses caused by deflection of the main stream in the manifolds into or out of the cells

The losses due to the deflection of main stream into or out of the cells are correlated to the flow and area ratios. This pressure loss can be determined from the following equations:

$$\Delta P_{c-in}[i] = 0.5 \cdot R_{c-in}[i] \cdot \rho \cdot U_{ch}[i]^2 \quad (5)$$

$$\Delta P_{c-out}[i] = 0.5 \cdot R_{c-out}[i] \cdot \rho \cdot U_{ch}[i]^2 \quad (6)$$

$$U_{ch}[i] = \frac{Q_c[i]}{z \cdot A_{ch}} \quad (7)$$

where $Q_c[i]$ is the coolant flow rate in the ith cooling flow field of the stack, $U_{ch}[i]$ is the coolant flow velocity in each channel of the cooling flow field, z is the number of channels in the cooling flow field, A_{ch} is the cross sectional area of each channel and $R_{c-in}[i]$ and $R_{c-out}[i]$ are the hydraulic resistances. As shown in Table 1, these hydraulic resistances are functions of the area ratio, the ratio between cross sectional area of a manifold and cross sectional area of all cooling channels in each cooling flow field, and the flow ratio.

2.1.4. Pressure losses related to the cooling flow field

As shown in Eq. (8a), the pressure drop related to the cooling flow field is mainly caused by different factors:

$$\Delta P_{cell}[i] = \Delta P_{ch}[i] + \Delta P_{c-in}[i] + \Delta P_{c-out}[i] \quad (8a)$$

$$\Delta P_{ch}[i] = \Delta P_{f-b}[i] + \Delta P_{en}[i] + \Delta P_{ex}[i] \quad (8b)$$

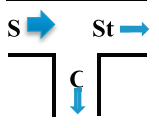
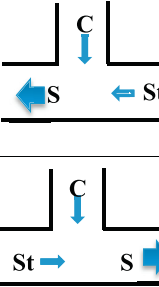
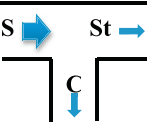
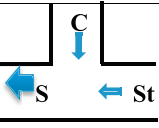
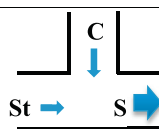
- a) Pressure drop due to friction losses in the flow field channels and rotation of the coolant flow through bending sections of the flow field channels (ΔP_{f-b})
- b) Pressure drop due to contraction and expansion of the coolant flow through T shape section between each cell and the corresponding manifold segment ($\Delta P_{en} + \Delta P_{ex}$)

A numerical simulation can be employed to characterize the pressure drop due to friction and bending losses (ΔP_{f-b}) in the cooling flow field. Therefore, a numerical model of the flow field is developed and run for a range of coolant flow rates. In this way a set of data including different coolant flow velocities and their corresponding pressure drops of the coolant across the flow field is obtained. The relationship between the pressure drop and the flow velocity is determined by fitting a second order polynomial to these data:

$$\Delta P_{f-b}[i] = AU_{ch}[i]^2 + BU_{ch}[i] \quad (9)$$

Table 1

Hydraulic resistance correlations of convergence and divergence of coolant flow in cells and manifolds [14].

	Shape of section	Derived or fitted equation	
Cell inlet		$R_{c_s_in}[i] = 725 \left(\frac{Q_c[i]}{Q_s[i]} \right)^6 - 1546 \left(\frac{Q_c[i]}{Q_s[i]} \right)^5 + 1267 \left(\frac{Q_c[i]}{Q_s[i]} \right)^4$ $- 497.7 \left(\frac{Q_c[i]}{Q_s[i]} \right)^3 + 98.49 \left(\frac{Q_c[i]}{Q_s[i]} \right)^2$ $+ 6.282 \left(\frac{Q_c[i]}{Q_s[i]} \right) + 1.765$ $R_{c_in}[i] = \frac{R_{c_s_in}[i]}{\left(U_c[i]/U_s[i] \right)^2}$	
Cell outlet		U & Z types	$R_{c_s_out}[i] = 1 + \left(\left(\frac{Q_c[i]}{Q_s[i]} \right) \left(\frac{A_c}{A_s} \right) \right)^2$ $- 2 \left(1 - \frac{Q_c[i]}{Q_s[i]} \right)^2$ $R_{c_out}[i] = \frac{R_{c_s_out}[i]}{\left(U_c[i]/U_s[i] \right)^2}$
Inlet manifold		$R_{s_st_in}[i] = -171.4 \left(\frac{Q_{st}[i]}{Q_s[i+1]} \right)^9 + 1266 \left(\frac{Q_{st}[i]}{Q_s[i+1]} \right)^8$ $- 3692 \left(\frac{Q_{st}[i]}{Q_s[i+1]} \right)^7 + 5729 \left(\frac{Q_{st}[i]}{Q_s[i+1]} \right)^6$ $- 5260 \left(\frac{Q_{st}[i]}{Q_s[i+1]} \right)^5 + 2966 \left(\frac{Q_{st}[i]}{Q_s[i+1]} \right)^4$ $- 1023 \left(\frac{Q_{st}[i]}{Q_s[i+1]} \right)^3 + 207.3 \left(\frac{Q_{st}[i]}{Q_s[i+1]} \right)^2$ $- 22.98 \left(\frac{Q_{st}[i]}{Q_s[i+1]} \right) + 1.697$ $R_{st_in}[i] = \frac{R_{s_st_in}}{\left(1 - \frac{Q_c[i+1]}{Q_s[i+1]} \right)^2} \times \frac{1}{(A_s/A_{st})^2}$	
Outlet manifold		U type	$R_{st_out}[i] = 13.5 \left(\frac{Q_c[i+1]}{Q_s[i+1]} \right)^5 - 2.9 \left(\frac{Q_c[i+1]}{Q_s[i+1]} \right)^4 + 25.7 \left(\frac{Q_c[i+1]}{Q_s[i+1]} \right)^3$ $- 5.6 \left(\frac{Q_c[i+1]}{Q_s[i+1]} \right)^2 - 0.4 \left(\frac{Q_c[i+1]}{Q_s[i+1]} \right) + 0.8$
		Z type	$R_{st_out}[i] = 13.5 \left(\frac{Q_c[i-1]}{Q_s[i-1]} \right)^5 - 2.9 \left(\frac{Q_c[i-1]}{Q_s[i-1]} \right)^4 + 25.7 \left(\frac{Q_c[i-1]}{Q_s[i-1]} \right)^3$ $- 5.6 \left(\frac{Q_c[i-1]}{Q_s[i-1]} \right)^2 - 0.4 \left(\frac{Q_c[i-1]}{Q_s[i-1]} \right) + 0.8$

where ΔP_{f-b} is the pressure drop of the coolant across the flow field of i th cell, U_{ch} is the mean velocity of the coolant in the channels which is obtained from the flow rates, and A and B are constants which are determined by curve fitting. The first order and the second order terms come from the friction losses and the channel bending, respectively.

Finally, the pressure drops due to expansion and contraction of the coolant flow at entrance and exit section of each cell are determined using the following relations:

$$\Delta P_{en}[i] = 0.5 \cdot R_{en} \cdot \rho \cdot U_{ch}[i]^2 \quad (10)$$

$$\Delta P_{ex}[i] = 0.5 \cdot R_{ex} \cdot \rho \cdot U_{ch}[i]^2 \quad (11)$$

where R_{en} and R_{ex} are hydraulic resistances due to expansion and contraction of the coolant flow in inlet and outlet portion of each cooling flow field channel [15].

2.1.5. Solution algorithm

The solution algorithm starts with an initial estimate of the coolant flow rate through the flow fields. A uniform flow distribution between different flow fields is assumed for the first

iteration step. Then, the coolant flow rates in different sections of the manifolds are determined. The local velocities in the manifolds and in the channels of the flow fields are computed knowing the flow rates. The different pressure drops are calculated using equations (1)–(11). The next step is to calculate the local pressures in the inlet and outlet manifolds. By assuming that the pressure at exit port of the stack is zero, the local pressures in the inlet and outlet manifolds are calculated. The pressure drops in the cooling flow fields can now be corrected by knowing the local pressures in the inlet and outlet manifolds. New cell flow rates are then calculated from the corrected coolant flow velocities in flow field channels using the following equation.

$$Q_{\text{corr}}[i] = U_{\text{corr}}[i] \cdot (zA_{\text{ch}}) \quad (12)$$

where $Q_{\text{corr}}[i]$ is the corrected flow rate of i th cell, $U_{\text{corr}}[i]$ is the corrected local velocity in the channels of the flow fields, z is the number of channels in the cooling flow field and A_{ch} is the cross sectional area of each channel.

Under relaxation of the cell flow rates, is also applied to ensure stable computation.

$$[Q_c[i]]_{j+1} = [Q_c[i]]_j + ([Q_{\text{corr}}[i] - Q_c[i]]_j)Fr \quad (13)$$

where $[Q_c[i]]_{j+1}$ is the new under relaxed flow rate of i th cell, j is the numerator of iteration and Fr is the under relaxation coefficient.

Once the new flow rates are obtained, they are compared with the initial guess or the previously calculated cell flow rates. The calculations continue with the new obtained set of cell flow rates until the differences between the new and old values (i.e. residuals) are become within the convergence criteria. Thus, the convergence criterion of coolant flow distribution submodel is the amount of residuals of cell coolant flow rates between two consecutive iterations which are calculated using the following equation.

$$\text{Residual} = \sum_{i=1}^{i=N} |[Q_c[i]]_{j+1} - [Q_c[i]]_j| \quad (14)$$

The final output of the coolant flow distribution model is the coolant flow distribution between different flow fields of the stack. A MATLAB code was developed using the above algorithm to determine the coolant flow distribution in the stack. A simplified

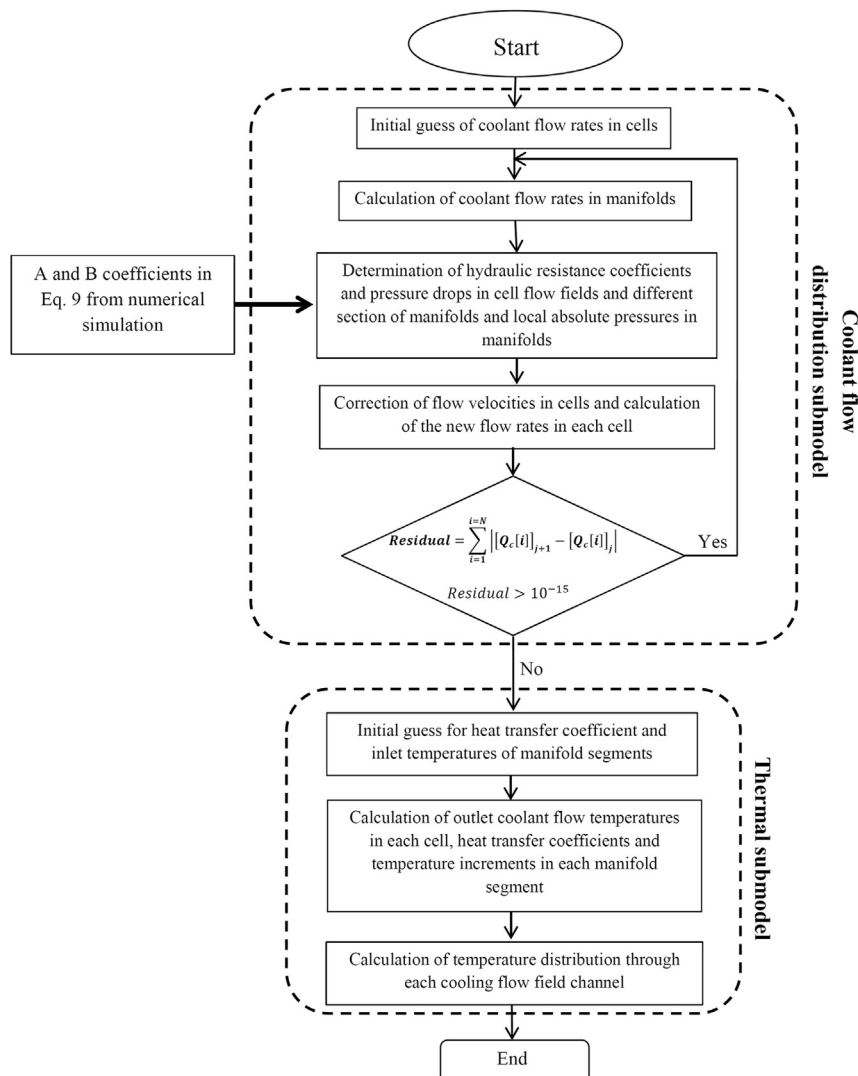


Fig. 2. Simplified solution algorithm of the coolant flow distribution and the thermal submodels.

scheme of the solution algorithm for coolant flow distribution submodel can be seen in Fig. 2.

2.2. Thermal submodel

The thermal submodel is developed to determine the temperature distribution in the stack. Within the framework of the present study, each cooling flow field can be considered as a parallel flow heat exchanger in which several channels of rectangular cross-section extend in parallel to each other from the inlet manifold to the outlet manifold and the heat is transferred from the cathode side of membrane electrode assemblies (MEA) to the coolant streams through bipolar plates. The analysis is based on the following assumptions:

1. Each cell in the stack has its own cooling flow field.
2. Heat transfer is steady state. Thus, heat generated in each cell is removed completely by the coolant and, therefore, the temperature distribution in the cell remains unchanged with time.
3. The heat generated by the electrochemical reaction in the cathode side of each cell transfers to its adjacent cooling flow field stream through the bipolar plates by conductive heat transfer. The reaction rate over the active area of the MEA is assumed to be uniform. This yields an approximately uniform heat generation over the cell's active area and, therefore, there is a constant heat flux at the walls of channels in the cooling flow field. By this assumption, the temperature distribution can be non-uniform over the active area in each individual cell in the stack.

The rate of heat generation per each cell in the stack at any working voltage can be determined using the following equation [12]:

$$Q[i] = (1.23 - V[i])I \quad (15)$$

where $Q[i]$, $V[i]$ and I are the rate of heat generation in i th cell, working voltage of i th cell, and output electrical current of the stack, respectively.

4. Neglecting the entrance effects, the coolant flow and the thermal conditions are assumed to be fully developed.
5. Thermal resistances at the surface of the cooling channels are negligible.
6. Viscous dissipation in the coolant flow is negligible.
7. Only heat transfer by conduction in the through-plane direction from the MEA to the cooling flow field is considered. Net conductive heat transfer in the in-plane directions in the bipolar plates is neglected.
8. The free convective heat transfer from the surfaces of the stack to the ambient air is negligible [7].
9. The amount of temperature increment at each manifold segment is calculated under an iterative procedure.

Each individual channel in the cooling flow field is modeled as a tube of rectangular cross section extending from the inlet manifold to the outlet manifold in parallel with other channels of the same flow field. The temperature distribution in the bipolar plate along the flow channels is determined using governing equations of internal flow in a tube with rectangular cross section and constant surface heat flux as following [16,17]:

$$T_s(x) = \frac{q_{ch}[i]}{hA_{sa}} + T_{ch-i}[i] + \frac{q_{ch}''[i]P}{\dot{m}_{ch}c_p}x \quad (16)$$

where h is the convection heat transfer coefficient, $q_{ch}[i]$ is the contribution of each flow field channel from the generated heat in

its related cell which is obtained by dividing the rate of heat generation in each cell, $Q[i]$, by the number of channels in the flow field, P is the perimeter of cross-section of the channel, A_{sa} is the surface area of each channel which is equal to product of the parameter, P , and the channel length, T_{ch-i} is the coolant temperature at inlet section of the flow field channel in each cell, $q_{ch}''[i]$ is the surface heat flux which is obtained by dividing the parameter $q_{ch}[i]$ by the surface area of the channel, x is the distance from the channel inlet along the channel, \dot{m}_{ch} is coolant mass flow rate in the channel obtained by dividing the cell mass flow rate by the number of channels in the cooling flow field.

The specific heat capacity of the coolant is assumed to be a function of temperature [18].

$$C_p[i] = a_1 \exp\left(-\frac{(T_m[i] - b_1)^2}{c_1}\right) + a_2 \exp\left(-\frac{(T_m[i] - b_2)^2}{c_2}\right) + a_3 \exp\left(-\frac{(T_m[i] - b_3)^2}{c_3}\right) + a_4 \exp\left(-\frac{(T_m[i] - b_4)^2}{c_4}\right) + a_5 \exp\left(-\frac{(T_m[i] - b_5)^2}{c_5}\right) \quad (17)$$

where $T_m[i]$ is mean of the inlet and outlet coolant temperatures in i th cooling flow field:

$$T_m[i] = \frac{T_{ch-i}[i] + T_{ch-o}[i]}{2} \quad (18)$$

The inlet coolant temperature, T_{ch-i} , is known and the outlet coolant temperature, T_{ch-o} , is determined by the following equation:

$$T_{ch-o}[i] = \frac{q_{ch}[i]}{\dot{m}_{ch}[i]C_p} + T_{ch-i}[i] \quad (19)$$

Since the specific heat capacity of the coolant varies with the mean temperature and the mean temperature is a function of cell outlet temperature which itself is unknown, thus the outlet coolant temperature and the specific heat capacity in each cooling flow field should be determined simultaneously by an iterative procedure.

A concept of Index of Uniform Temperature (IUT) was proposed by Chen et al. to evaluate the degree of uniform temperature profile



Fig. 3. PEM fuel cell system used in the experimental tests.

across the cooling plates [19]. In the present study, a modified form of this index is introduced as:

$$IUT = \frac{\sum_{i=1}^N \sum_{j=1}^M |T(i,j) - \bar{T}|}{N \times M}, \quad \bar{T} = \frac{\sum_{i=1}^N \sum_{j=1}^M T(i,j)}{N \times M} \quad (20)$$

where N is the number of cooling flow fields in the stack, M the number of nodes taken along the cooling channel from the inlet manifold to the outlet manifold, \bar{T} is the average temperature of the stack and $T(i,j)$ is the local temperature in bipolar plate at i th cooling flow field and j th node. With regard to the definition of this index in equation (20), its value decreases as the degree of temperature uniformity within the stack increases. A simplified scheme of the solution algorithm for the thermal submodel can be seen in Fig. 2.

3. Experimental

In the current research, a series of experimental tests were conducted in order to build confidence in the model. The tests were performed using a home-made PEMFC system (Fig. 3). The PEMFC system contains 2 stacks. While the stacks are electrically connected in series, the coolant and the reactant gases are delivered to them in parallel. One of the stacks has a U-configuration flow pattern, and the other one has a Z-configuration flow pattern. Each stack contains 65 cells with a cell active area equal to 225 cm². The MEA consists of NRE-211 membrane, catalyst layer with a total Pt loading of 0.4 mg cm⁻² at both the anode and cathode sides and SGL carbon cloth with micro porous layer as the gas diffusion layer (GDL). A more detailed description of the anode and the cathode flow fields can be found in our previous work [7].

The cooling flow field was of parallel serpentine pattern including 10 channels with cross section of 3 mm × 2 mm. The coolant inlet and outlet manifolds were of the same shape and size with cross section of 5 cm × 3 cm.

Fuel and oxidant subsystems deliver hydrogen and air at a constant stoichiometry of 1.2 and 2.0, respectively. Hydrogen and air are humidified up to 95% relative humidity prior to entering the fuel cell stacks. Operating pressures of the anode and the cathode sides were kept constant at 0.4 bar (g) and 0.3 bar (g), respectively. Unutilized fuel from the anode exhaust is recirculated back to the feed stream via a recirculation pump.

During the tests, the coolant temperature at the inlets of both stacks was kept constant in the 49 °C, with the total coolant flow rate of 52 L min⁻¹. Therefore, each stack approximately received 26 L min⁻¹ of the total coolant flow rate. The total coolant flow rate and inlet pressure of the stacks were measured via a digital flow meter and a pressure transducer, respectively. The flow meter was gpi TM075-N, ¾ in and the pressure transducer was of Wikai type A-10.

A series of temperature measurement tests were carried out on the stacks. Since determination of temperature distribution within the bipolar plates was impossible during fuel cell stack operation, it was decided to measure the temperature distribution along the bipolar plate edges instead. Temperature measurements were made using a “DT-9875 Thermal Imager” infrared thermal camera.

4. Results and discussion

The model was constructed based on the homemade U and Z shape stacks to analyze the thermal behavior of these stacks and also to verify the model's predictions by the experimental results. In other words, the geometrical characteristics and working conditions of the stacks are used as input parameters for the model.

The PEM fuel cell stacks considered for the simulation contain 65 cells with 225 cm² active cell area. The inlet and the outlet manifold dimensions are assumed to be 3 cm × 5 cm. Unless otherwise stated, it is assumed that there is a uniform cell voltage distribution through the stack. The current density at working condition is assumed to be 1.0 A cm⁻² at 0.6 V per each cell. The cooling flow field is of modified parallel serpentine shape. Table 2 lists a summary of input parameters, dimensions and properties of the fuel cell stacks used in the present model.

Another input parameter of the model is the flow rate– pressure drop characteristic of the cooling flow field as described previously (Eq. (11)) which obtained via a numerical model. The numerical model was composed of 10 channels of rectangular cross-section of 2 mm × 3 mm extend in parallel to each other from the inlet manifold to the outlet manifold. Inlet and outlet boundary conditions of the model were assumed to be the mass flow inlet and the pressure outlet, respectively. The number of meshes for the model was totally equal to 1,446,025 hexahedral cells. A series of numerical simulations were performed to characterize the variations of coolant pressure drop across the cooling flow field as a function of mean velocity of the coolant in the channels (Eq. (11)). The values obtained for A and B are 10,543 (Ns² m⁻⁴) and 1728.6 (Ns m⁻³), respectively. An example of the contour plot of pressure drops obtained for 0.4 L min⁻¹ of coolant flow rate per cell is depicted in Fig. 4.

Fig. 5 shows the overall coolant flow distribution between different cells in the U and Z-shape stacks. As seen from Fig. 5, there is a non-uniform flow distribution in both stacks. The U-shape stack shows a gradually increasing flow distribution along the stack while the flow distribution in the Z-shape stack is of parabola type. The range of variations in cell flow rates in the Z-shape and the U-shape stacks are about 0.21 L min⁻¹ and 0.12 L min⁻¹, respectively. The standard deviations of cell flow rates are computed as 0.0619 and 0.0325 for the U and Z configurations, respectively. Therefore, it seems that the Z-shape stack has a more uniform coolant flow distribution than the U-shape stack.

Fig. 6 shows contour plots of temperature distribution in the stacks with U and Z configurations. The contour plots show a symmetric parabola temperature distribution for the Z configuration and an increasing temperature distribution for the U configuration. The temperature is minimum near the stack inlet and increases as the distance from the inlet increases. There is a uniform temperature distribution in the stacks at the local points near to the inlet but the temperature non-uniformity prevails at the local points far away from the inlet. The values of IUT are computed as

Table 2

Parameters and properties of the fuel cell stacks used in the present simulations.

Component	Parameters	Symbols	Value
Cooling flow field	Cooling channel dimensions	A_{ch}	3 mm × 2 mm
	Channel length	A_{sal}/P	0.56 m
	Number of channels	z	10
	Number of turns		3
	Constant A in Eq. 9	A	10,543
	Constant B in Eq. 9	B	1728.6
Coolant	Flow rate per stack		26 L min ⁻¹
	Inlet temperature		49 °C
	Density	ρ	982 kg m ⁻³
	Dynamic viscosity	μ	464×10^{-3} N s m ⁻²
	Conduction coefficient		655.3 N m ² K ⁻¹
Stack	Number of cells	N	65
	Cell active area		225 cm ²
	Manifold dimensions	A_m	5 cm × 3 cm
	Manifold length for each cell	L	1 cm
	Cell voltage	$V[i]$	0.6 V
	Stack output current	I	220 A

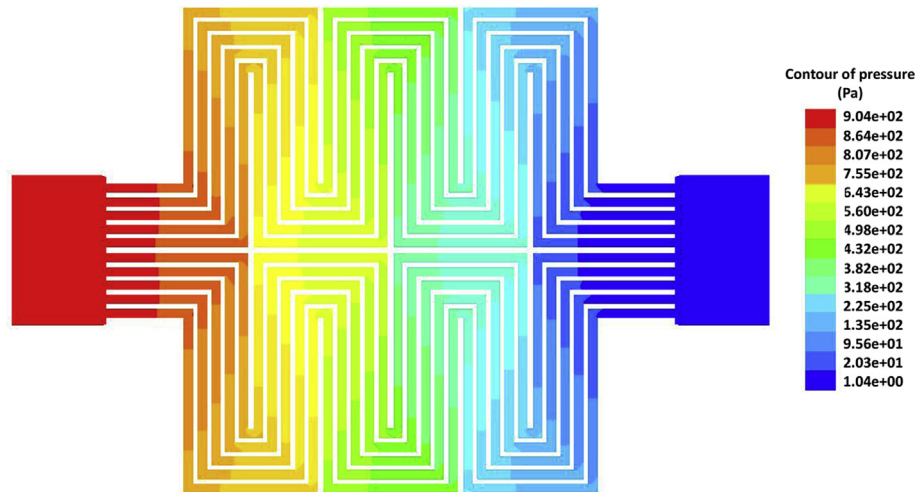


Fig. 4. Contour plot of pressure distribution in the cooling flow field.

1.30 and 1.26 for the U and Z configurations, respectively. Since the value of IUT for the Z configuration is lower than that of U configuration, the Z configuration can result in a more uniform temperature distribution in a stack with the above mentioned geometrical specifications.

4.1. Verification of the simulation results

The PEM fuel cell system was run under the same conditions as those considered for the simulation (Table 2). A series of temperature measurement tests were carried out on the stacks. As stated before, since measurement of temperature distribution within the bipolar plates was not possible during the fuel cell stack operation

by common methods; it was decided instead to measure the temperature distribution along the vertical and horizontal surfaces of the stacks.

In this part of the study, the non-uniformity of cell voltages was taken into account in the simulations in order to increase the precision of the model. Therefore, experimentally measured voltages of the cells during the tests were used as the input parameters of the model. In Fig. 7 a bar graph of cells' voltage distribution for the U and Z configurations is illustrated. The infrared pictures of the two stacks under operation are shown in Fig. 8. The inlet manifolds are at the bottom and the exit manifolds are at the top. Furthermore, the horizontal direction of coolant flow in the stacks is shown by the arrows in Fig. 8. As seen from these photos, the regions near

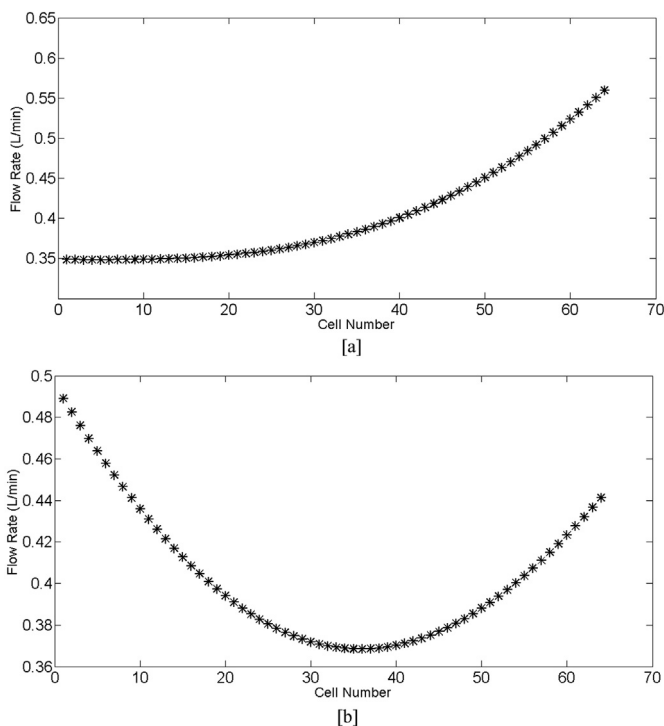


Fig. 5. Coolant flow distribution in the stacks; (a) U configuration and (b) Z configuration.

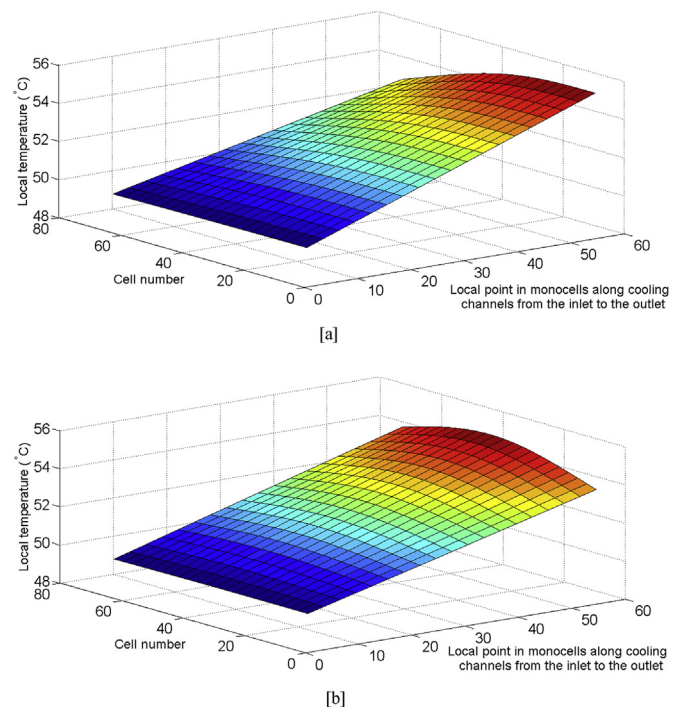


Fig. 6. Contour plot of temperature distribution within the stacks; (a) U configuration and (b) Z configuration.

to the inlet manifolds have lower temperatures than the regions near to the exit manifolds. Additionally, in the stack with the Z configuration, temperature is higher at the middle region of the stack. This is due to the fact that the cells located in this region receive lower coolant flow rates. But in the stack with U configuration, the temperature is lower at the cells located near to the inlet port of the stack, because these cells receive higher flow rates of the coolant. Moreover, in these pictures, some hot points are observed on the faces of the stacks which lead to some fluctuations in temperature readings. The cause of forming such hot points is explained in the next paragraphs.

In Fig. 9, the temperature variations along the centerline of the upper face of the stack close to the exit coolant manifold obtained from experimental measurements are compared to those obtained by the simulation. A reasonably good agreement between the simulation results and the experimental data can be observed. As seen from Fig. 9, temperature profiles show an increasing distribution along the stack for the U configuration and an approximately parabola distribution for the Z configuration.

The fluctuations seen in the model's predictions come from an uneven experimentally measured voltage distribution between different cells in the stack which result in an uneven heat generation. But the origin of high fluctuations in the experimental results is different. The experimental data have been extracted from

infrared pictures by a software. Since bipolar plates have been fabricated by machining of composite blanks, there are some color variations on bipolar faces and edges. These color variations lead to different emissions and different temperature readings. Therefore, high fluctuations in experimental data are not real and just come from color variations on the bipolar surfaces.

It is worthy of notice that Pei et al. have also found such a parabolic temperature distribution in their Z shape stack [20]. They measured the temperature distribution experimentally and concluded that the temperature differences in the stack exhibited a parabola distribution at different current densities.

Fig. 10 shows the comparison between the numerically and experimentally obtained temperature variations along the vertical edges of two certain cells in the U shape stack from region near to the inlet manifold to region near to the outlet manifold. One of these cells is located in the middle of the stack (Fig. 10a) and the other one is located close to one end of the stack where coolant inlet and outlet ports are placed in (Fig. 10b). As seen from this figure, there is a reasonably good agreement between the simulation results and the experimental data. As expected, the temperature in any point on the edge which is near to the exit manifold is higher than that of its corresponding point near to the inlet manifold. This is due to the fact that the coolant temperature at the exit region of cooling flow field is higher than that of the inlet

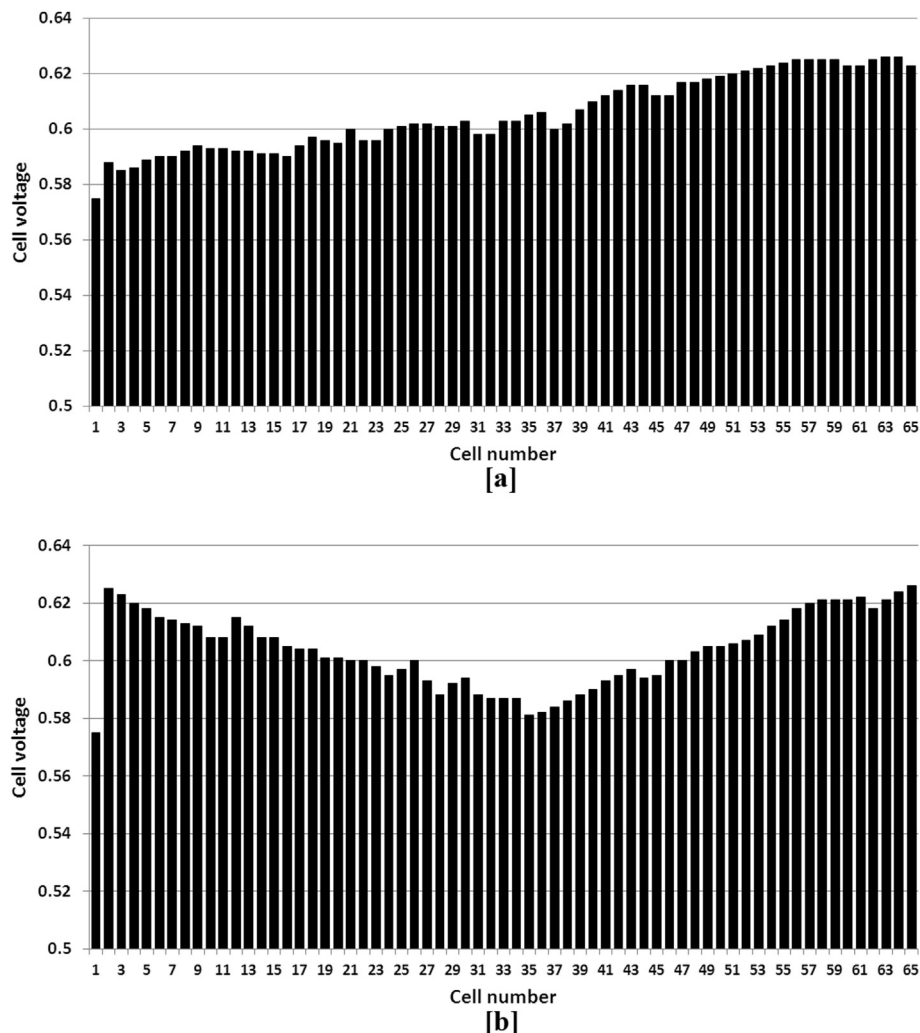


Fig. 7. Cells' voltage distribution; (a) U configuration and (b) Z configuration.

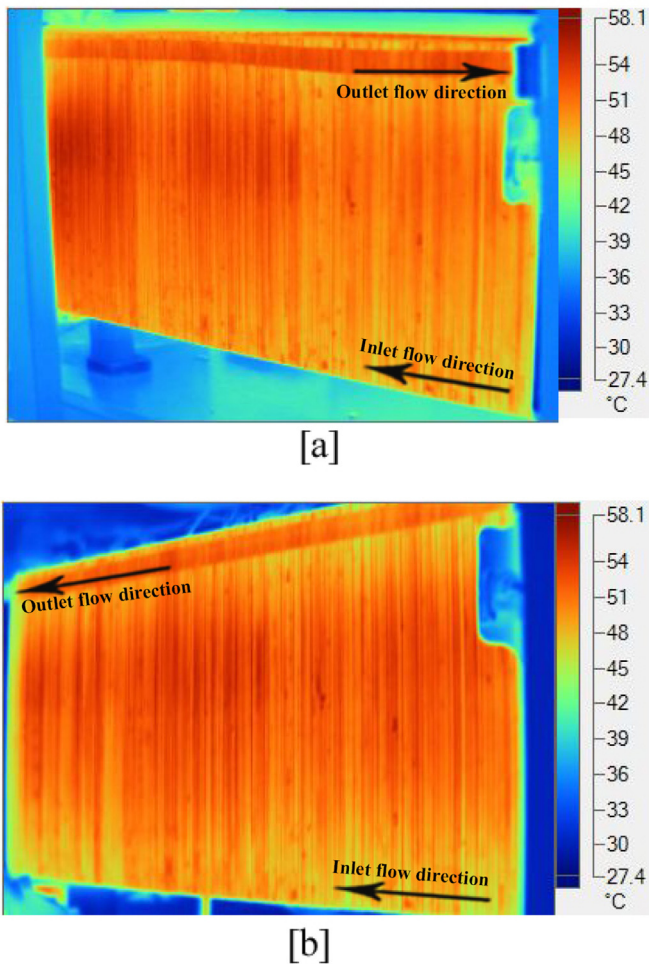


Fig. 8. Infrared pictures of the stacks; (a) U configuration and (b) Z configuration.

region; therefore, temperature of the bipolar plate at this region should be higher in order to maintain uniform heat flux.

As discussed above, comparison of the simulation results with the available experimental data shows that the proposed model can reasonably predict the thermal response of a PEM fuel cell stack. However, more experimental measurements and data are required to improve the accuracy of the model. For example, designing an experimental setup to measure the coolant flow distribution between different cells in a stack can be advantageous for improving the precision of the hydraulic resistance relations and therefore the accuracy of the coolant flow distribution submodel.

4.2. Parametric analysis

In the previous sections, it was stated that maintaining uniform coolant flow and temperature distributions within a PEM fuel cell stack are desired. These distributions are affected by some parameters like: size of the inlet and outlet manifolds, flow distribution pattern in cells and size of the flow channels, coolant flow rate, etc. For example, sufficient temperature distribution uniformity can be achieved through an enlarged manifold and reduced flow channel sizes. However, excessively small flow channels can lead to excessive pumping power required to drive the coolant flow, in addition to other problems such as manufacturing difficulty. Optimal cooling of a stack can be attained by optimizing the size of the manifold and flow channels as well as the coolant flow rate.

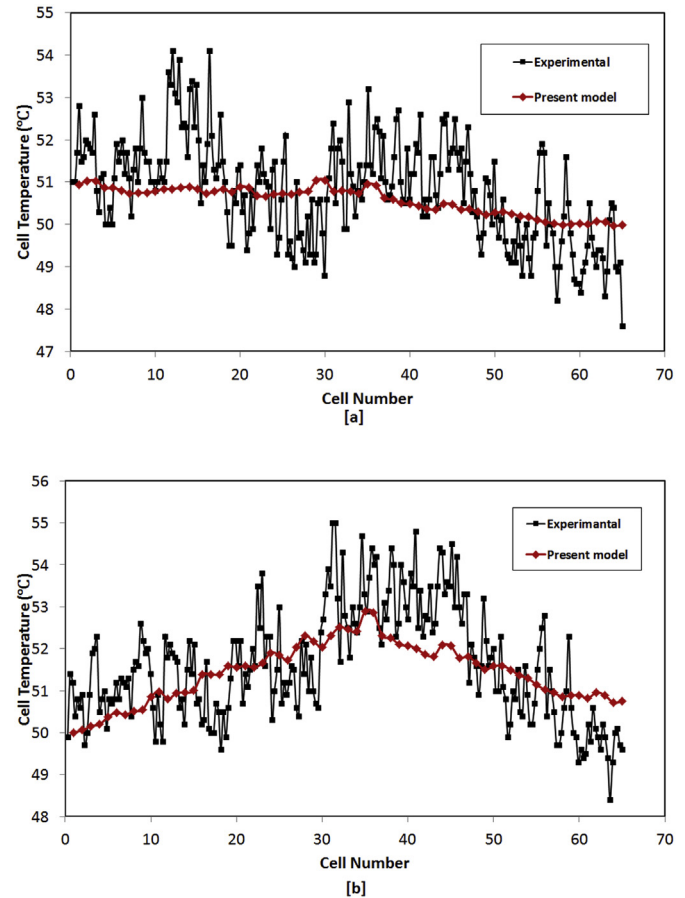


Fig. 9. Comparison of temperature variations along the centerline of the upper face of the stack close to the exit coolant manifold from the simulation and experiments at the nominal working conditions; (a) U configuration and (b) Z configuration.

A parametric study is conducted to investigate the effects of the manifold size and the coolant flow rate on the temperature distribution in a PEM fuel cell stack.

4.2.1. Manifold size

The cross sectional area of the inlet and outlet manifolds of a stack has a considerable effect on the coolant flow distribution between different cells in the stack. Hence, the degree of temperature uniformity within the stack is affected by the manifolds sizes. As a simplifying assumption, the inlet and outlet manifolds are assumed to be the same size. Unless otherwise stated, the input parameters for the simulations are the same as those presented in Table 2. A uniform cell voltage distribution is also considered through the stacks.

In Fig. 11, the IUT is compared between the U and Z configurations for the various cross sectional area of the manifolds. With regard to the definition of IUT, its value decreases as the degree of temperature uniformity within the stack increases. The Z configuration results in more uniform temperature distribution than the U configuration in low values of the cross sectional area. However, at the larger values, both configurations result in the same temperature uniformity. It can be explained by the fact that the pressure losses in the manifolds increase as the cross sectional area decreases. On the other hand, coolant distribution between cells becomes more non-uniform by increasing pressure losses in the manifolds while keeping the pressure losses in the cells constant.

Much smaller manifold sizes were not considered in the current analysis, because during the analysis of the Z configuration stack, it

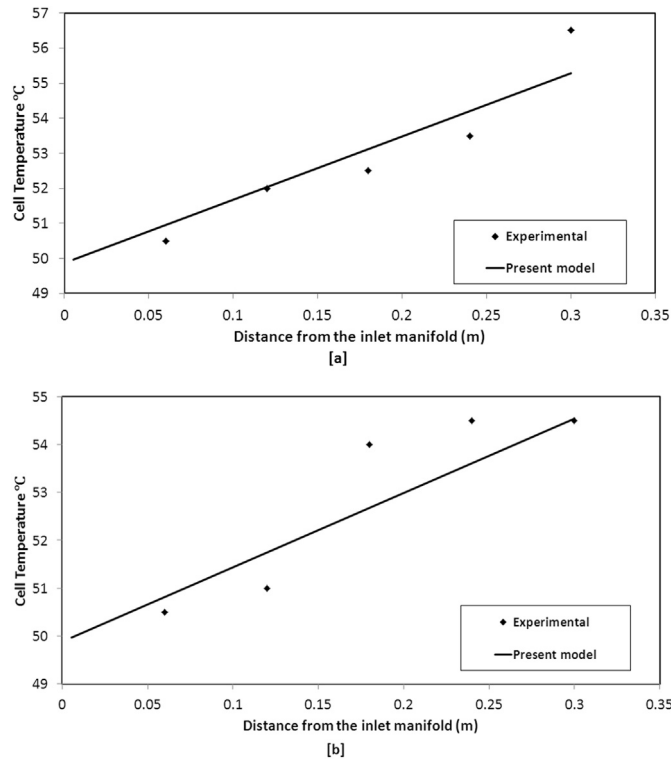


Fig. 10. Temperature profiles along vertical edges of two certain cells; (a) cell located in the middle of the stack and (b) cell located close to the inlet of the stack.

was revealed that the very small manifold sizes lead to backflow in some middle cells due to excessive pressure drop in the inlet and outlet manifolds. The resulting backflow causes hot coolant in the outlet manifold to stream into the cell cooling flow field and finally pour into the inlet manifold. Hence, overheating of those cells which experience the backflow is inevitable. The occurrence of backflow in the case of small manifold sizes was also confirmed in a special pipe flow network analysis software through a simplified model of Z configuration stack.

4.2.2. Effect of total coolant flow rate

Fig. 12 depicts the effect of coolant flow rate on the temperature uniformity in the stacks. As expected, the value of IUT decreases by

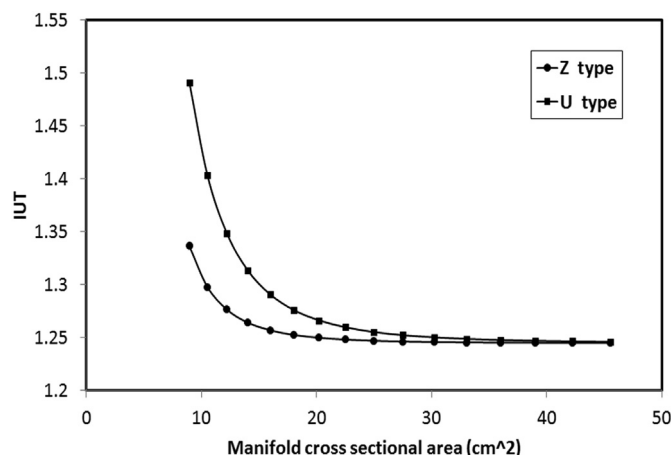


Fig. 11. Comparison of IUT between the stacks with the U and the Z configurations.

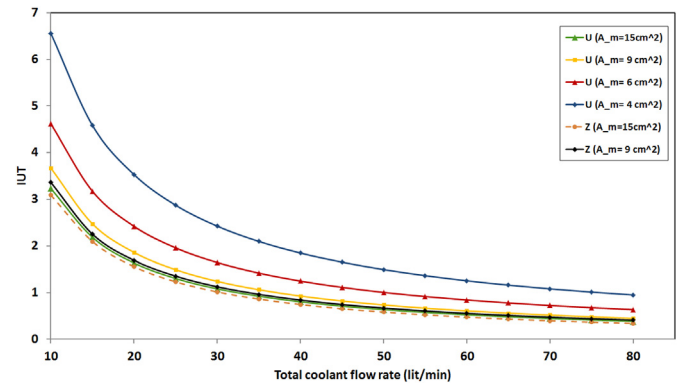


Fig. 12. Effect of coolant flow rate on the temperature uniformity.

increasing the coolant flow rate; however, the rate of decrease is larger at the lower flow rates and manifold cross sectional areas. This trend is less significant in the Z configuration than the U configuration. Regarding to uniform temperature distribution criteria, it is beneficial to increase the coolant flow rate as much as possible, whereas higher coolant flow rate leads to higher parasitic power due to coolant pumping. Thus, a trade-off between maximum temperature uniformity and minimum parasitic losses due to excessive coolant pumping determines optimized amount of total coolant flow rate. Moreover, in the whole of coolant flow range, the IUT in the Z configuration is lower than that of the U configuration with the same manifold cross sectional area. Thus, the Z configuration results in a more uniform temperature. It should be noted that, the smaller manifold sizes were not considered for Z configuration, as they causes backflow in some middle cells.

5. Conclusion

In the present study, a non-isothermal mathematical model was introduced for investigation of thermal management in PEM fuel cell stacks. The model was formed by two main submodels, a coolant flow distribution submodel and a thermal submodel. Two common stack configurations were compared to each other with assistance of the model. The results depicted that the degree of temperature uniformity is more in the Z configuration than the U configuration. Simulation results were verified by comparing experimentally measured temperature profiles along the vertical and horizontal edges of the bipolar plates with those obtained by the analytical model. A parametric analysis was also conducted to determine the effects of various factors on the stack temperature uniformity. Among miscellaneous parameters, the manifold size and the coolant flow rate were selected to investigate their effects on the temperature uniformity in the stacks. A modified form of standard deviation was also introduced as an index of uniform temperature. In addition, the following results were obtained:

- 1 The degree of temperature uniformity within the stack increases as the cross sectional area of the inlet and outlet manifolds increase. The Z configuration results in more uniform temperature distribution than the U configuration in low values of the manifold cross sectional area. However, at the larger values, both configurations result in the same temperature uniformity.
- 2 The value of IUT decreases as the coolant flow rate increases. The rate of reduction in IUT is larger at the lower flow rates. On the other hand, higher coolant flow rate leads to higher parasitic power due to coolant pumping. Thus, optimized amount of total

coolant flow rate is determined by compromising between maximum temperature uniformity and minimum parasitic losses due to excessive coolant pumping.

Acknowledgment

The authors would like to acknowledge the financial support of Renewable Energy Organization of Iran (SUNA).

References

- [1] A.M. López-Sabirón, J. Barroso, V. Roda, J. Barranco, A. Lozano, F. Barreras, *Int. J. Hydrogen Energy* 37 (2012) 7289–7298.
- [2] S. Kang, K. Min, F. Mueller, J. Brouwer, *Int. J. Hydrogen Energy* 34 (2009) 6749–6764.
- [3] G. Zhang, S.G. Kandlikar, *Int. J. Hydrogen Energy* 37 (2012) 2412–2429.
- [4] X. Li, *Platin. Met. Rev.* 50 (2006) 200–201.
- [5] S.G. Kandlikar, Z. Lu, *Appl. Therm. Eng.* 29 (2009) 1276–1280.
- [6] M. Ji, Z. Wei, *J. Energies* 2 (2009) 1057–1106.
- [7] S. Asghari, H. Akhgar, B.F. Imani, *J. Power Sources* 196 (2011) 3141–3148.
- [8] Y. Zhang, M. Ouyang, Q. Lu, J. Luo, X. Li, *Appl. Therm. Eng.* 24 (2004) 501–513.
- [9] S. Yu, D. Jung, *Renew. Energy* 33 (2008) 2540–2548.
- [10] A.P. Sasmito, E. Birgersson, A.S. Mujumdar, *Int. J. Hydrogen Energy* 36 (2011) 12991–13007.
- [11] J. Park, X. Li, *J. Power Sources* 162 (2006) 444–459.
- [12] J. Larminie, A. Dicks, M.S. McDonald, *Fuel Cell Systems Explained*, second ed., John Wiley & Sons, Chichester, 2003.
- [13] A. Faghri, Z. Guo, *Int. J. Heat Mass Transfer* 48 (2005) 3891–3920.
- [14] I.E. Idelchik, E. Fried, *Handbook of Hydraulic Resistance*, third ed., Jaico Publishing House, India, 2005.
- [15] R.W. Fox, A.T. McDonald, P.J. Pritchard, *Introduction to Fluid Mechanics*, seventh ed., John Wiley & Sons, New York, 2008.
- [16] F. Incropera, D. DeWitt, *Introduction to Heat Transfer*, fifth ed., John Wiley & Sons, New York, 2006.
- [17] S. Kakaç, R.K. Shah, W. Aung, *Handbook of Single-Phase Convective Heat Transfer*, first ed., John Wiley & Sons, New York, 1987.
- [18] Osborne, Stimson, Ginnings, *Handbook of Chemistry and Physics*, 53rd ed., 1973, Cleveland, Ohio.
- [19] F.C. Chen, Z. Gao, R.O. Loutfy, M. Hecht, *Fuel Cells* 3 (2003) 181–188.
- [20] H. Pei, Z. Liu, H. Zhang, Y. Yu, Z. Tu, Z. Wan, W. Liu, *J. Power Sources* 227 (2013) 72–79.